HAL
open science

Flows instabilities analysis using a reduced dynamic mode decomposition method

Frédéric Lévy

To cite this version:

Frédéric Lévy. Flows instabilities analysis using a reduced dynamic mode decomposition method. 2023. hal-03034486v4

HAL Id: hal-03034486

https://hal.science/hal-03034486v4

Preprint submitted on 21 Dec 2023

HAL is a multi-disciplinary open access archive for the deposit and dissemination of scientific research documents, whether they are published or not. The documents may come from teaching and research institutions in France or abroad, or from public or private research centers.

L'archive ouverte pluridisciplinaire **HAL**, est destinée au dépôt et à la diffusion de documents scientifiques de niveau recherche, publiés ou non, émanant des établissements d'enseignement et de recherche français ou étrangers, des laboratoires publics ou privés.

Flows instabilities analysis using a reduced dynamic mode decomposition method

Frédéric Lévy
DMPE, ONERA, Université Paris Saclay, F-91123 Palaiseau, France

The equivalence between dynamic mode decomposition and discrete Fourier transform for numerical and experimental data, the mean of which in each set equals zero, is used to propose an analytical solution for the DMD, which is equivalent to the equations for the DFT. This solution is an exact solution, based on the reduction of all the snapshots by the mean of the whole sequence, which is also the rigid mode (not time dependant) of the considered sequence. The sampling time step is assumed to be constant. The time dependant evolution of the modal shapes is a linear combination of all the reduced snapshots, the weight functions being the results of the analytical solution. The frequency of each mode remains constant in the time. This simple solution allows to process in a quite short time a great amount of data, the limit of which is the computer RAM size. This analysis method offers to bring out better the preponderant modes and to make continuous videos of the selected modes shapes. This paper presents an application of this reduced DMD method to an academic validation case, typically unsteady and transient, dealing with 50000 snapshots and 125000 values per snapshot.

I. Introduction

BASED on the Koopman analysis of nonlinear dynamical systems [1], the « dynamic mode decomposition » technique was introduced by Rowley et al. [2] and Schmid [3], as a numerical procedure for extracting dynamical features from flow data. DMD computes a set of modes, the frequency of which remains constant in the time. The method highlights the major periodic phenomena, and permits to reconstruct the signal by choosing the most representative modes. It is based on data (experimental or CFD results) whose equations generating them are not known a priori. The modes are not orthogonal between each other, but their time dependant evolution can be physically meaningful.

To extract the dynamic features of the snapshots, some important matrix processings, such as the QR decomposition [3, 4, 5], or the Single Value Decomposition [3, 6, 7] are commonly used. However, they require

some advanced resolution techniques as well as some important computer resources. The efficient and accurate method proposed by Drmac et al. [8] does not mention any information about this last point, but it is not unreasonable to think this method requires some important computer resources as well.

In this supplementary analysis using DMD, the choice was made to find a resolution method which sets free from any matrix processing, and to reduce significantly the computing time, in particular when the snapshots number and the values number per snapshot are high. A few years after the introduction of the DMD, Chen et al. [9] have outlined a possibility to subtract the snapshots mean to all the snapshots, and they showed this operation leads to an exact reduction of the DMD to the temporal discrete Fourier transform. Although they mentioned this result is undesirable, explaining the implications of the mean subtraction, this operation is used here again, assuming the sampling time step is constant, to extract frequencies and spatial structures from fluid mechanics data. The notion of modal growth rate is therefore abandoned.

On the other hand, the obtained analytical solution is an exact solution. The time dependant evolution of the modal shapes is a linear combination of all the reduced snapshots, the weight functions being the results of the analytical solution. The frequency of each mode remains constant in the time. No matrix processing is required to describe the modal behaviour of the sequence. The error of this DMD analysis solution comes only from the data themselves : the time step, the snapshots number, and the snapshots values. This simple solution allows to process in a quite short time a great amount of data, the limit of which is the computer RAM size. Dealing with a great number of snapshots allows to compensate some disadvantages outlined for the DFT, to bring out better the preponderant modes and to make continuous videos of the selected modes shapes. Other authors who had an interest in zero-mean data used for DMD have based their work on Chen et al.'s document [11-13].

In the next paragraph, the analytical solution of this modified DMD method is proposed, and some arguments to compensate some disadvantages are presented. The aim of this paper is to validate the method through its application to an academic case, typically unsteady and transient, with 50000 snapshots and 125000 values per snapshot.

II. Theoretical reminder

The solution of the DMD method in this paper is based on a definition of DMD as an algorithm applied to a sequential snapshot set. It is not the most general definition of DMD, which was written by Tu [10], but is often useful for theoretical analyses.

A. Method description

$N + 1$ snapshots are considered : $\boldsymbol{v}_0, \boldsymbol{v}_1, \boldsymbol{v}_2, ..., \boldsymbol{v}_N$. A vector $\boldsymbol{v}_j$ stands for the field of a variable which describes the calculated flow or the experimental data at the instant of index j ($0 \leq j \leq$ N). As it is mentioned in quite a lot of articles, the mean value of all the snapshots, a vector noted $\bar{\boldsymbol{v}}$, is introduced [3, 7, 9-17] :

$$\bar{\boldsymbol{v}} = \frac{\sum_{i=0}^{N} \boldsymbol{v}_i}{N+1} \tag{2.1}$$

The relation (2.1) is written again in order to bring out the subtraction of the mean vector to all the snapshots [9, 16] :

$$\boldsymbol{v}_N - \bar{\boldsymbol{v}} = N\bar{\boldsymbol{v}} - \sum_{i=0}^{N-1} \boldsymbol{v}_i = -\sum_{i=0}^{N-1} \left(\boldsymbol{v}_i - \bar{\boldsymbol{v}}\right) \tag{2.2}$$

This operation is then equivalent to consider only the fluctuations of the snapshots around the mean value, which depends on the sequence itself, since it may change if the considered time interval changes. Defining the matrix $\boldsymbol{D}_0^{N-1}$ and $\boldsymbol{D}_1^{N}$ as $\boldsymbol{D}_0^{N-1} = \left\{\boldsymbol{v}'_0, \boldsymbol{v}'_1, \boldsymbol{v}'_2, \ldots, \boldsymbol{v}'_{N-1}\right\}$ and $\boldsymbol{D}_1^{N} = \left\{\boldsymbol{v}'_1, \boldsymbol{v}'_2, \ldots, \boldsymbol{v}'_{N-1}, \boldsymbol{v}'_N\right\}$, with $\boldsymbol{v}'_i = \boldsymbol{v}_i - \bar{\boldsymbol{v}}$, the relation (2.2) can be synthesized into the expression :

$$\boldsymbol{D}_1^{N} = \boldsymbol{D}_0^{N-1} \boldsymbol{S} \tag{2.3}$$

$\boldsymbol{S}$ is a companion type square matrix :

$$\boldsymbol{S} = \begin{pmatrix} 0 & \cdots & \cdots & 0 & -1 \\ 1 & 0 & & \vdots & -1 \\ 0 & 1 & \ddots & \vdots & \vdots \\ \vdots & \ddots & \ddots & 0 & -1 \\ 0 & \cdots & 0 & 1 & -1 \end{pmatrix}_{N,N} \tag{2.4}$$

The DMD analysis is based on the spectral decomposition of the companion matrix, which appears here to be very simple, since the eigenvalues of $\boldsymbol{S}$ are the (N+1)st roots of unity, excepted unity. The expression for the eigenvalues, noted λ_p , is determined such as the argument is included between $-\pi$ and π ($-\pi$ excluded), to let appear the conjugate eigenvalues. An integer m is introduced : if N is even, $m = \frac{N}{2}$. If N is odd, $m = \frac{N-1}{2}$. The constant sampling time step Δt is used to link the eigenvalues to the modal frequencies.

For $p = 0$ to $m - 1$, $$\lambda_p = \exp\left(\frac{2i\pi\,(p-m)}{N+1}\right) \tag{2.5}$$

The associated frequency is : $$f_p = \frac{p-m}{(N+1)\Delta t} \tag{2.6}$$

For $p = m$ to $N - 1$, $$\lambda_p = \exp\left(\frac{2i\pi\,(p+1-m)}{N+1}\right) \tag{2.7}$$

The associated frequency is : $$f_p = \frac{p+1-m}{(N+1)\Delta t} \tag{2.8}$$

Since $-\pi < \omega_p\,\Delta t \le \pi$, with $\omega_p = 2\pi\, f_p$, then the maximal frequency is : $$f_{\max} = \frac{1}{2\Delta t} \tag{2.9}$$

The resolution frequency Δf is expressed as : $$\Delta f = \frac{1}{(N+1)\Delta t} \tag{2.10}$$

The tolerance around a modal frequency is $\Delta f / 2$.

A left eigenvector basis of $\boldsymbol{S}$ is a Vandermonde matrix, noted $\boldsymbol{V}$, made up from the eigenvalues of $\boldsymbol{S}$:

$$\boldsymbol{V}\boldsymbol{S} = \boldsymbol{\Lambda}\boldsymbol{V} \tag{2.11}$$

with $$\boldsymbol{V} = \begin{pmatrix} 1 & \lambda_0 & \lambda_0^2 & \cdots & \lambda_0^{N-1} \\ 1 & \lambda_1 & \lambda_1^2 & \cdots & \lambda_1^{N-1} \\ \vdots & \vdots & \vdots & & \vdots \\ 1 & \lambda_{N-1} & \lambda_{N-1}^2 & \cdots & \lambda_{N-1}^{N-1} \end{pmatrix} \tag{2.12}$$

$\boldsymbol{\Lambda}$ is the eigenvalues matrix : $\boldsymbol{\Lambda} = \mathrm{diag}(\lambda_0, \ldots , \lambda_{N-1})$. The elements can be linked with time since the sampling time step is constant. In that case, the Vandermonde matrix columns are linked to a time dependant evolution, while the lines are linked to a modal evolution [6]. Since the eigenvalues of the companion matrix are simple, the Vandermonde matrix is invertible. Therefore, the decomposition of the companion matrix is :

$$\boldsymbol{S} = \boldsymbol{V}^{-1}\boldsymbol{\Lambda}\boldsymbol{V} \tag{2.13}$$

To calculate the expression of the elements of the Vandermonde matrix inverse, which are noted b_{ij}, the matrix $\boldsymbol{V}^{-1}$ is written as a right eigenvector basis of the matrix $\boldsymbol{S}$:

$$\boldsymbol{S}\boldsymbol{V}^{-1} = \boldsymbol{V}^{-1}\boldsymbol{\Lambda} \tag{2.14}$$

Then this property is developed. Multiplying the relation (2.14) on the right by the unit vector $\boldsymbol{e}_j$ of the $(j + 1)^{th}$ column, some relations are derived between the elements of the column of index j of the matrix $\boldsymbol{V}^{-1}$. $\boldsymbol{S}\left(\boldsymbol{V}^{-1}\boldsymbol{e}_j\right)=\boldsymbol{V}^{-1}\left(\boldsymbol{\Lambda}\,\boldsymbol{e}_j\right)$ is equivalent to :

$$\begin{pmatrix} 0 & 0 & \cdots & 0 & -1 \\ 1 & 0 & & \vdots & -1 \\ 0 & 1 & \ddots & \vdots & \vdots \\ \vdots & \ddots & \ddots & 0 & -1 \\ 0 & \cdots & 0 & 1 & -1 \end{pmatrix} \times \begin{pmatrix} b_{0,j} \\ b_{1,j} \\ \vdots \\ b_{N-2,j} \\ b_{N-1,j} \end{pmatrix} = \lambda_j \begin{pmatrix} b_{0,j} \\ b_{1,j} \\ \vdots \\ b_{N-2,j} \\ b_{N-1,j} \end{pmatrix} \tag{2.15}$$

The relation (2.15) yields : $\quad 0 \le i \le N\text{-}1 \qquad b_{ij} = b_{N-1,j} \times \dfrac{\lambda_j^{N-i} - 1}{\lambda_j - 1}$ (2.16)

As the relation (2.16) gives the coefficients b_{ij} by a constant, the identity $\boldsymbol{V}\boldsymbol{V}^{-1} = \boldsymbol{I}$ is used to provide the closure relation :

$$\sum_{k=0}^{N-1} \lambda_i^k \, b_{kj} = \delta_{ij} \qquad (\delta_{ij} \text{ is the Kronecker symbol}) \tag{2.17}$$

Knowing that $\lambda_p^{N+1} = 1$, the elements b_{ij} of the matrix $\boldsymbol{V}^{-1}$ (line index i = 0 to N-1, column index j = 0 to N-1) are deduced :

$$\boxed{b_{ij} = \frac{\lambda_j\left(\lambda_j^{N-i} - 1\right)}{N+1}} \tag{2.18}$$

The identities $\boldsymbol{V}\boldsymbol{V}^{-1} = \boldsymbol{I}$ and $\boldsymbol{V}^{-1}\boldsymbol{V} = \boldsymbol{I}$ can be checked with the help of the relations $\sum_{k=0}^{N-1} \lambda_p^k = -\dfrac{1}{\lambda_p}$ with (p = 0 to N-1), and $1 + \sum_{k=0}^{N-1} \lambda_k^q = 0$ with $0 < |q| \le N$.

B. Modal Matrix

Combining the relations (2.3) and (2.14), appears the matrix $\boldsymbol{W} = \boldsymbol{D}_0^{N-1}\boldsymbol{V}^{-1}$, allowing to write the matrix $\boldsymbol{D}_1^N$ as the product :

$$\boldsymbol{D}_1^N = \boldsymbol{W}\,\boldsymbol{\Lambda}\,\boldsymbol{V} \tag{2.19}$$

The columns of $\boldsymbol{W}$ are noted $\boldsymbol{w}_p$ (p = 0 to N-1) :

$$\boldsymbol{w}_p = \sum_{k=0}^{N-1} \boldsymbol{v}'_k \, b_{kp} = \sum_{k=0}^{N-1} \boldsymbol{v}'_k \, \frac{\lambda_p \left(\lambda_p^{N-k} - 1\right)}{N+1} \qquad \text{with} \quad \boldsymbol{v}'_k = \boldsymbol{v}_k - \overline{\boldsymbol{v}} \tag{2.20}$$

The relation (2.19) is equivalent to the expression :

For j = 0 to N-1,

$$\sum_{p=0}^{N-1} \boldsymbol{w}_p \, \lambda_p^{j+1} = \boldsymbol{v}'_{j+1} \tag{2.21}$$

At the time t = 0, associated with j = -1 in the relation (2.21), the identity $\boldsymbol{V}^{-1}\boldsymbol{V} = \boldsymbol{I}$ is used.

$$\boldsymbol{V}^{-1}\boldsymbol{V} = \boldsymbol{I} \quad \Leftrightarrow \quad \sum_{k=0}^{N-1} b_{ik} \, \lambda_k^j = \delta_{ij} \tag{2.22}$$

$$\sum_{p=0}^{N-1} \boldsymbol{w}_p = \sum_{p=0}^{N-1} \left(\sum_{k=0}^{N-1} \boldsymbol{v}'_k \, b_{kp} \right) = \sum_{k=0}^{N-1} \boldsymbol{v}'_k \left(\sum_{p=0}^{N-1} b_{kp} \right) = \sum_{k=0}^{N-1} \boldsymbol{v}'_k \, \delta_{k0} = \boldsymbol{v}'_0 \tag{2.23}$$

The vector $\boldsymbol{w}_p$ is the complex shape of the mode $_p$ at the time t = 0. Since the matrix $\boldsymbol{W}$ contains all the vectors $\boldsymbol{w}_p$, it can be named a modal matrix.

C. Time dependant evolution of the modes

Using the matrix $\boldsymbol{W}$ and $\boldsymbol{\Lambda}$, the whole time dependant evolution of the snapshots can be rebuilt. In particular for one specific mode, if it is preponderant in front of other modes. In that case, since the components of the final shapes are real values, the time dependant evolution of the shape of the mode p, the eigenvalue of which λ_p is complex, must be computed with the time dependant evolution of the shape of the mode q, where λ_q is the conjugate eigenvalue of λ_p. If $\lambda_q = \overline{\lambda}_p$, then $b_{kq} = \overline{b}_{kp}$ and $\boldsymbol{w}_q = \overline{\boldsymbol{w}}_p$. The column of index q in $\mathbf{V}^{-1}$ is the conjugate column of the column of index p. As a result, the vector $\boldsymbol{w}_p \, \lambda_p^j + \boldsymbol{w}_q \, \lambda_q^j$, the elements of which are real, represents the total contribution of the mode at the positive frequency f_p (relation (2.8)) at the time of index j (j = 0 to N). The amplitude of the mode p at the instant j is the Euclidean norm of this vector.

$$\boldsymbol{w}_p \, \lambda_p^j + \boldsymbol{w}_q \, \lambda_q^j = 2 \, \mathrm{Re}\left(\boldsymbol{w}_p \, \lambda_p^j\right) = \frac{2}{N+1} \left(\sum_{k=0}^{N-1} \boldsymbol{v}'_k \, \mathrm{Re}\left(\lambda_p^{j-k} - \lambda_p^{j+1}\right) \right) \tag{2.24}$$

The time dependant evolution of the shape of the mode p, the pulsation of which is $\omega_p = 2\pi \, f_p$, is given eventually by the expression :

$$\boxed{\boldsymbol{w}_p \, \lambda_p^j + \boldsymbol{w}_q \, \lambda_q^j = \frac{2}{N+1} \left(\sum_{k=0}^{N-1} \boldsymbol{v}'_k \left(\cos\left(\omega_p \left(j-k\right)\Delta t\right) - \cos\left(\omega_p \left(j+1\right)\Delta t\right) \right) \right)} \tag{2.25}$$

Or, with $t_j = j\,\Delta t$ ($j = 0$ to N) and :

$$\boxed{\boldsymbol{w}_p\,\lambda_p^j + \boldsymbol{w}_q\,\lambda_q^j = \frac{2}{N+1}\left(\sum_{k=0}^{N-1}\boldsymbol{v}'_k\left(\cos\left(\omega_p\left(t_j - t_k\right)\right) - \cos\left(\omega_p\left(t_j + \Delta t\right)\right)\right)\right)} \tag{2.26}$$

The time dependant evolution of the modal shapes is obtained directly from the reduced snapshots, weighted by a simple time dependant function. Therefore it is not necessary to calculate the Vandermonde matrix, its inverse, and the modal matrix. The amplitude of the mode of frequency f_p at the time t_j is still the Euclidean norm of the vector given by the relation (2.25).

D. Comments

The eigenvalues are completely independent of the data. They depend only on the snapshots number, and the spectral resolution is uniform, like the one obtained by a discrete Fourier transform. This is a result for a DMD analysis made on fluctuating data (removing the mean of the original data), which is usually considered as a disadvantage, compared to a DMD analysis made on the raw data (without subtracting the mean), leading to a non-uniform spectral resolution [3, 6, 9]. In both cases, the resolution frequency decreases with an increase of the snapshots number. The value of a modal frequency is necessarily associated with a tolerance around this value, because the real value may not be usually exactly predicted. With a unique resolution frequency, the tolerance is very simple (half of the resolution frequency). In order to approach the real value of a modal frequency, the tolerance must decrease. Increasing the snapshots number is a convenient possibility. Increasing the sampling time step is not relevant, because some information about the researched physical phenomena can be lost.

By construction of the eigenvalues, the Nyquist condition is implicitly respected. The mean-subtraction sets free from any constraint about a minimum number of snapshots, since the method works regardless of the number and the values of the snapshots. In practice, a DMD analysis leads of course to a much better result with a high number of snapshots (see section III). With this DMD method equivalent to DFT, the solution is an exact solution, since the coefficients of the last column of the companion matrix $\mathbf{S}$ are all equal to -1. No more matrix processing is required to get the results. This analytical solution sets completely free from the constraint to operate such processings, which are expensive in time calculation and in memory size if N is high. The error of this DMD analysis method comes only from the data themselves : the time step, the snapshots number, and the snapshots values. This simple solution processes in a short time a quite great amount of data, the limit of which is the computer RAM size.

The notion of amplified or damped modes, as it is common in the original DMD analysis, does not exist here, since all the eigenvalues have a unit magnitude. The obtained modes are just preponderant or not. We must keep in mind that the notion of modal growth rate is valid only in the time window of the data sequence, since the calculation does not know what happens physically before the first snapshot and after the last one. Whatever the original DMD method can reveal about this dynamical information, it is limited in the time of the observed data. In addition, with the original DMD method, it is known that the local frequency resolution around the frequency of interest depends both on the snapshots number and the last snapshot [6, 9]. This last snapshot strongly influences the quality of the DMD analysis, and no rules can be deduced for an appropriate choice of the snapshot sequence and the frequency resolution [6]. This problem does not arise with this DMD method equivalent to DFT. Therefore, it is not unreasonable to turn towards a method, although equivalent to DFT, which presents some other significant advantages, as long as the right preponderant modes of any sequence are still detected.

In the end, the great advantage of the DMD is the possibility to make visible the time dependant evolution of the shapes of the selected preponderant modes. The time dependant evolution of a mode is equivalent to a time dependant deformation of its initial shape to a certain frequency with an optional phase shift.

An validation example of a typical unsteady and transient case treated with this DMD method is presented in section III. It comes out its preponderant modes are determined correctly.

III. Application to an academic validation case

E. Context

The DMD code, built with the analytical solution, is tested to find the acoustic modes of a 2D cavity. The cavity is rectangular. The length (1 m) is noted L, the width (50 cm) is noted h (figure 1). It is closed at one extremity in the length direction (at the abscissa origin), and open at the other one. It is filled with still air at ambient conditions. A pressure impulse is introduced at the initial instant within the cavity, and the waves propagation and reflections which develop inside are observed. This case is typically unsteady and transient, since the pressure impulse vanishes while the additional mass contained in the impulse is evacuated gradually at the exit on the right side of the cavity, until the ambient pressure is reached everywhere inside the cavity (theoretically at the end of an infinite time).

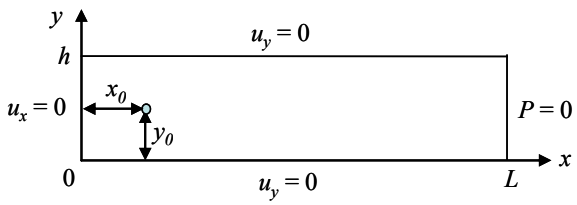

Fig. 1 Schema of the 2D cavity

The central position of the pressure impulse is on the median line of the cavity at $y_0 = h / 2$ and at $x_0 = 2$ cm from the left wall. The impulse pressure is applied in a 8 mm square centred at the point (x_0 , y_0) and oriented like the rectangle of the cavity. The fluid is inviscid and non turbulent.

F. Theoretical solution

Without any friction during the waves propagation, the flow remains isentropic. Therefore, the classical governing equations linearized for small perturbations (the second order terms are neglected) in a still fluid are [18] :

$$\Delta P - \frac{1}{c_0^2}\frac{\partial^2 P}{\partial t^2} = 0 \quad \text{and} \quad \frac{\partial \mathbf{v}}{\partial t} = -\frac{1}{\rho_0}\nabla P \tag{3.1}$$

The pressure P and the velocity $\mathbf{v}$, the components of which are noted u and v, represent the small perturbations around their mean values. The mean pressure is the ambient pressure. The mean velocity vector is null. Therefore, the mean density ρ_0 and the sound velocity c_0 are constant ($c_0 = 347.2$ m/s). The boundary conditions are :

$x = 0$ $\quad u = 0 \Leftrightarrow \partial P / \partial x = 0$

$x = L$ $\quad P = 0$

$y = 0$ and $y = h$ $\quad v = 0 \Leftrightarrow \partial P / \partial y = 0$

The pressure perturbation inside the cavity is then expressed in the form of a series of modes with two integers (n, p), the frequency of which is noted $f_{n,p}$ [18] :

$$P(x,y,t) = \sum_{n,p\geq 0} A_{n,p}\cos(\omega_{n,p}\,t)\cos\left(\left(n+\frac{1}{2}\right)\frac{\pi x}{L}\right)\cos\left(\frac{p\pi y}{h}\right) \tag{3.2}$$

$$\text{with} \quad \omega_{n,p} = 2\pi\, f_{n,p} \quad \text{and} \quad \boxed{f_{n,p} = \frac{c_0}{2}\sqrt{\frac{(2n+1)^2}{4L^2}+\frac{p^2}{h^2}}} \tag{3.3}$$

The theoretical frequencies of the 13 first acoustic modes of the cavity are written in the table 1. The $A_{n,p}$ coefficients are calculated on one side by integrating the pressure shape at the initial instant within the whole cavity

with the space weight functions of the relation (3.2), and on the other side, by using the orthogonality property of these weight functions in their space integration within the cavity [18]. The initial pressure impulse, noted δP, is 1000 Pa (about 1 % of the ambient pressure). The square side, where δP is applied, is noted 2 ε (thus $\varepsilon = 4$ mm). The expression of the $A_{n,p}$ coefficients is eventually :

if $p = 0$, $$A_{n,0} = \frac{4\,\varepsilon\,\delta P}{h}\,\mathrm{g}(n) \tag{3.4}$$

if p is even and $p > 0$, $$A_{n,p} = \frac{4\,\delta P\,(-1)^{p/2}\sin\left(\frac{p\,\pi\,\varepsilon}{h}\right)}{p\,\pi}\,\mathrm{g}(n) \tag{3.5}$$

with $$\mathrm{g}(n) = \frac{4\,\sin\left(\left(n+\frac{1}{2}\right)\frac{\pi\,\varepsilon}{L}\right)\cos\left(\left(n+\frac{1}{2}\right)\frac{\pi\,x_0}{L}\right)}{\left(n+\frac{1}{2}\right)\pi} \tag{3.6}$$

if p is odd, $A_{n,p} = 0$

G. DMD analysis applied to the theoretical solution

A structured mesh is used. The cell size in both directions is 2 mm, which leads to 500 cells in the longitudinal direction and 250 cells in the transversal direction. To match the results of a CFD finite-volume code which was used afterwards for comparisons, the pressure values given by the relation (3.2) are cell-centred. Thus, each snapshot intended to the DMD analysis has 125000 values. The 8 mm square, centred at the point (x_0 , y_0) and defined to receive the impulse pressure, contains therefore 16 cells around this point. Since 20 cells are usually required, in CFD computation using 2-order space schemes, to seize a wave length, this mesh is adapted to describe fluctuations up to 8680 Hz. To capture properly the physical phenomena which will be detected by the DMD analysis, the sampling time step Δt is 4 µs. The frequency resolution Δf for the DMD analysis is set at 5 Hz, which is quite small. Therefore, 50000 snapshots, linked here with the pressure field, must be stored ($N = 49999$), the final time of the calculation is 200 ms, and the maximal frequency which can be detected by the DMD analysis is 125 kHz. Only the modes below 1250 Hz are studied. All the DMD analysis calculations realized for this paper were operated on a computer, each processor of which contains 24 cores Broadwell Intel® Xeon® CPU E5-2650 v4 @ 2.20GHz, a RAM of 128 GB and a total crest power of 844 GFlops.

The pressure fluctuations, given by the relation (3.2), with the parameters values fixed in section F, were analysed. Since the convergence of the terms in the relation (3.2), as a function of the mode frequency, towards the complete theoretical solution is very slow, only the 157 modes below 5000 Hz in the relation (3.2) were computed,

which is quite enough considering the maximal frequency of the studied DMD modes. A size of 46.73 GB in the computer RAM and a CPU time of 7h 28mn 44s were required to compute 50000 instants of the truncated theoretical solution until 200 ms, immediately followed by the amplitudes of 250 DMD modes below 1250 Hz. The figure 2 shows the modal amplitudes of the pressure fluctuations at $t = 0$. The selection of the preponderant modes is made only by visual observation : the amplitude of a preponderant mode is higher than the amplitude of its neighbouring modes. Here, the figure 2 shows clearly some amplitude peaks, indicating the preponderant modes. Below 1250 Hz, 13 preponderant modes appear. The modes the peak of which is not so high as the others indicate a significant phase shift at $t = 0$ (their maxima appear later during their own period). The frequencies of the theoretical acoustic modes in the 2D cavity (relation (3.3)), and the frequencies detected by the DMD analysis of the truncated theoretical solution are written in the table 1. The time dependant shape of a mode is the same as the one defined by the term of the corresponding frequency in the relation (3.2).

The DMD frequencies of the computed theoretical solution equal exactly the theoretical frequencies, under the tolerance $\Delta f / 2$ (2.5 Hz). In consequence, the DMD analysis with the exact analytical solution, equivalent to DFT, works properly to detect the right preponderant modes.

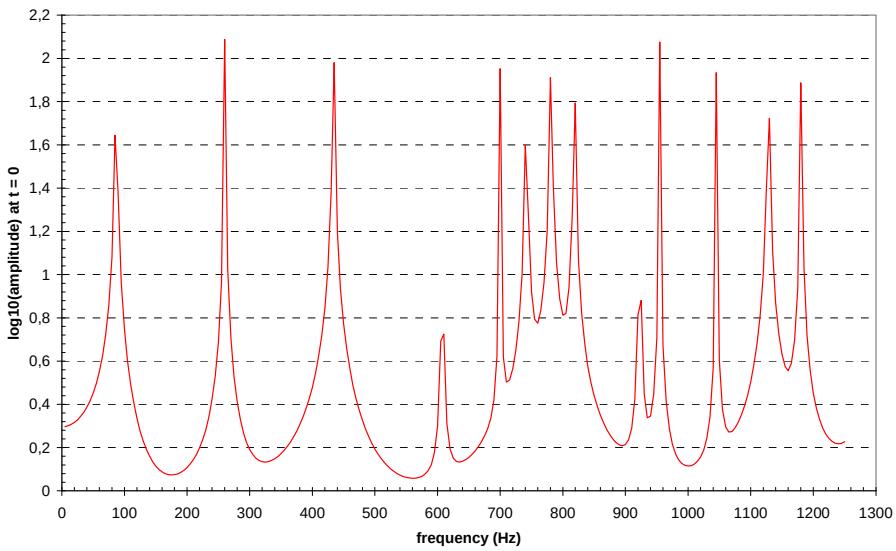

Fig. 2 Modal amplitudes of the pressure fluctuations theoretical solution at t = 0

Table 1 Acoustics modes frequencies in the 2D cavity

theoretical frequencies (Hz)	n	p	DMD frequencies theoretical solution (Hz)	$f_{DMD,TS} - f_{th}$ (Hz)	DMD frequencies CFD flow (Hz)	$f_{DMD,CFD} - f_{DMD,TS}$ (Hz)	$f_{DMD,CFD} / f_{DMD,TS}$ (%)
86.8	0	0	85	-1.8	85	0	0
260.4	1	0	260	-0.4	255	-5	-1.923
434	2	0	435	1	425	-10	-2.299
607.6	3	0	610	2.4	595	-15	-2.459
699.804	0	2	700	0.196	685	-15	-2.143
741.62	1	2	740	-1.62	725	-15	-2.027
781.2	4	0	780	-1.2	765	-15	-1.923
818.87	2	2	820	1.13	800	-20	-2.439
922.697	3	2	925	2.303	905	-20	-2.162
954.8	5	0	955	0.2	935	-20	-2.094
1045.21	4	2	1045	-0.21	1025	-20	-1.914
1128.4	6	0	1130	1.6	1105	-25	-2.212
1180.608	5	2	1180	-0.608	1155	-25	-2.119

H. CFD flow calculation

The code CEDRE [19, 20] developed at ONERA, was used to compute the flow in the cavity with a CFD code, in order to see any difference with the theoretical solution in the DMD analysis results. The mesh is described in section G (the computed quantities are cell centred). For this application, only the Euler equations were integrated by this finite-volume type code. No turbulence model. The Euler fluxes were discretized with the second-order HLLC scheme and a hybrid type limiter, which is the default standard model in CEDRE. The extrapolation to the interfaces was carried out on the natural variables. The temporal scheme was an explicit two-steps Runge-Kutta scheme, second order accurate. The time step was 2 µs (CFL = 0.35). As the sampling time step is 4 µs, the results were stored every two iterations. The boundary conditions were a wall condition at the top, bottom and left sides of the cavity, and a constant pressure (1 bar) at the right side. At the initial instant, the cavity contained still air at ambient conditions, with the same pressure impulse described in sections E, F and G. However, the temperature inside the impulse pressure was adapted in order to make the impulse entropy at the initial instant equal to the entropy outside the impulse. These conditions are the most adapted to get results which are the closest to the theoretical solution. A parallel computation with 64 numerical sub-domains, on the same computer mentioned in section G, took less than 30 minutes to calculate the flow until 200 ms.

First, the CFD results were converted to 50 000 pressure files in a specific format used to read the data for the DMD analysis. This operation took about 3h 30mn on the same computer described in section G. Then, the DMD program, which works sequentially, required a size of 46.57 GB in the computer RAM and a CPU time of 47mn 04s

to compute the amplitudes of 250 DMD modes below 1250 Hz. A specific time can be derived, with a view to estimate the CPU time of other modal amplitudes calculations, including files reading and writing :

$$t_{spec} = \frac{\text{CPU time}}{n_m \times n_s \times n_v} = \frac{2824 \text{ s}}{250 \times 50\,000 \times 125\,000} = 1.807\ 10^{-9} \text{ s} \tag{3-7}$$

n_m = number of considered modes ;

n_s = snapshots number ;

n_v = values number per snapshot.

The figure 3 shows the modal amplitudes of the pressure fluctuations at $t = 0$. Both cases are drawn, to highlight better the differences. Again, below 1250 Hz, 13 preponderant modes appear for the CFD flow, by visual observation of the amplitude peaks. The modes the peak of which is not high indicate a significant phase shift at $t = 0$ (their maxima appear later during their own period). However, a frequency gap between the preponderant modes of the CFD flow and the ones of the theoretical solution appears, and increases with the modes frequency. The frequencies detected by the DMD analysis of the CFD results are written in the table 1.

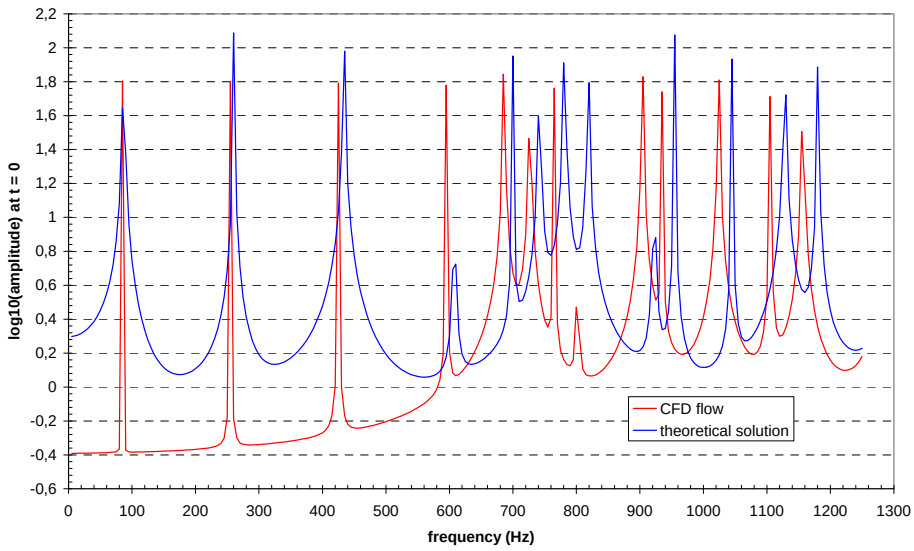

Fig. 3 Modal amplitudes of the validation case at t = 0

If the gap between the DMD modes frequencies of the CFD flow and of the theoretical frequencies increases with the frequency, their relative differences remain roughly constant from the second longitudinal mode (about -2.1 %). These differences show the CFD flow is not the same as the ideal flow, from which the relation (3.2) derives. The code CEDRE is non linear, the CFD flow has a compressible nature, the mean velocity is not necessarily zero everywhere and the boundary conditions involve a special processing of the whole variables describing the flow. The theoretical frequencies are derived from linearized equations, assuming the mean flow incompressible and still, and the boundary conditions concern only the pressure and velocity fluctuations [18]. It is not the purpose of this paper to investigate further the issue.

The modals shapes of the CFD flow are presented on the figure 4. The instants, extracted within the modes periods, are chosen in order to show the deformations at their maximum. The shapes are in good agreement with what is expected, with respect to the modal shapes of the theoretical solution.

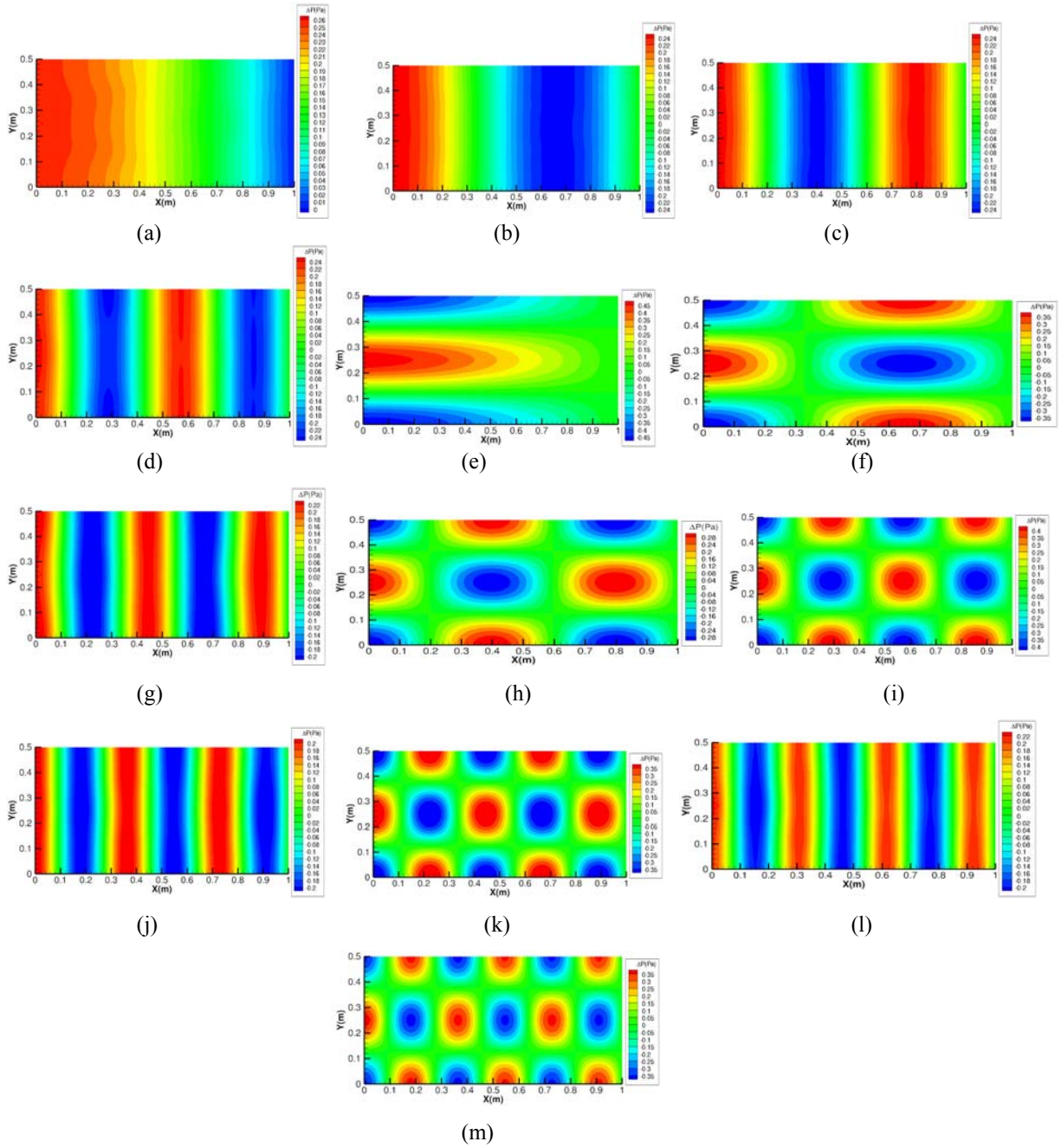

Fig. 4 (a) f = 85 Hz, mode 1L, t = 11.752 ms. (b) f = 255 Hz, mode 2L, t = 3.908 ms. (c) f = 425 Hz, mode 3L, t = 2.340 ms. (d) f = 595 Hz, mode 4L, t = 1.664 ms. (e) f = 685 Hz, mode 2T, t = 1.332 ms. (f) f = 725 Hz, mode 2L-2T, t = 1.132 ms. (g) f = 765 Hz, mode 5L, t = 1.288 ms. (h) f = 800 Hz, mode 3L-2T, t = 0.948 ms. (i) f = 905 Hz, mode 4L-2T, t = 0.108 ms. (j) f = 935 Hz, mode 6L, t = 1.044 ms. (k) f = 1025 Hz, mode 5L-2T, t = 0.088 ms. (l) f = 1105 Hz, mode 7L, t = 0.876 ms. (m) f = 1155 Hz, mode 6L-2T, t = 0.720 ms.

IV. CONCLUSION

The equivalence between dynamic mode decomposition and discrete Fourier transform for numerical and experimental data, based on the reduction of all the snapshots by the mean of the whole sequence, was used to propose an analytical and exact solution for the DMD, which is equivalent to the equations for the DFT. The sampling time step is assumed to be constant. The time dependant evolution of the modal shapes is a linear combination of all the reduced snapshots, the weight functions being the results of the analytical solution. This solution sets completely free from the constraint to operate matrix processings, which are expensive in time calculation and in memory size if the snapshots number is high. The eigenvalues of the companion matrix are completely independent of the data. They depend only on the snapshots number, and the spectral resolution is uniform. The Nyquist condition is implicitly respected. The tolerance associated with the spectral resolution is half of the resolution frequency. In order to approach the real value of a modal frequency, the tolerance must decrease. Increasing the snapshots number is a convenient possibility, but not the sampling time step, because some information about the researched physical phenomena can be lost. The notion of amplified or damped modes, as it is common in the original DMD analysis, does not exist here, since all the eigenvalues have a unit magnitude. The obtained modes are just preponderant or not, keeping in mind that the notion of modal growth rate is valid only in the time window of the data sequence, since the calculation does not know what happens physically before the first snapshot and after the last one. Whatever the original DMD method can reveal about the dynamical information, it is limited in the time of the observed data. Therefore, it is not unreasonable to turn towards a method, although equivalent to DFT, which presents some other significant advantages, as long as the right preponderant modes of any sequence are still detected. This method is valid regardless of the number and the values of the snapshots. The error of this DMD analysis solution comes only from the data themselves : the time step, the snapshots number, and the snapshots values. This simple solution allows to process in a quite short time a great amount of data, the limit of which is the computer RAM size. The great advantage of the DMD is the possibility to make visible the time dependant evolution of the shapes of the selected preponderant modes. Dealing with a great number of snapshots allows, in one hand, to compensate some disadvantages outlined for the DFT, and on the other hand, to bring out better the preponderant modes and to make continuous videos of the selected modes shapes.

An academic validation case, typically unsteady and transient, dealing with 50000 snapshots and 125000 values per snapshot, was presented in this paper. The theoretical solution of this case was obtained with the classical

governing equations linearized for small perturbations in a still fluid. The DMD analysis with the reduced method was applied to the computed theoretical solution, showing the DMD frequencies of this solution equal exactly the theoretical frequencies, under the tolerance frequency. Therefore, the DMD analysis with the exact analytical solution, equivalent to DFT, works properly to detect the right preponderant modes. Then the flow of the academic case was computed with a CFD code developed at ONERA, in order to see any difference with the theoretical solution in the DMD analysis results. The conditions used for this calculation were the most adapted to get results which are the closest to the theoretical solution. A gap, increasing with the frequency, appears between the DMD modes frequencies of the CFD flow and of the theoretical frequencies. But their relative differences remain roughly constant and small from the second longitudinal mode. These differences show the CFD flow is not exactly the same as the ideal flow, from which the theoretical solution derives. However, the modals shapes of the CFD flow are in good agreement with what is expected, with respect to the modal shapes of the theoretical solution.

REFERENCES

[1] Koopman, B. O., "Hamiltonian systems and transformations in Hilbert space", *Proceedings of the National Academy of Sciences of the United States of America*, Vol. 17, No. 5, 1931, pp. 315–318.

[2] Rowley, C. W., Mezic, I., Bagheri, S., Schlatter, P., Henningson, D. S.,"Spectral analysis of nonlinear flows", *Journal of Fluid Mechanics,* Vol. 641, 2009, pp. 115–127.

[3] Schmid, P. J.,"Dynamic mode decomposition of numerical and experimental data", *Journal of Fluid Mechanics,* Vol. 656, 2010, pp. 5–28.

[4] Francis, J. G. F., *The QR transformation – A unitary analogue to the LR transformation – part 1,* 1961, URL: http://comjnl.oxfordjournals.org/content/4/3/265.full.pdf

[5] Francis, J. G. F., *The QR transformation – part 2,* 1961, URL: http://comjnl.oxfordjournals.org/content/4/4/332.full.pdf

[6] Richecoeur, F., Hakim, L., Zimmer, L., "Décomposition en Modes Dynamiques - Présentation et illustrations", Laboratoire EM2C, CNRS UPR 288, Ecole Centrale Paris, 2012.

[7] Richecoeur, F., Hakim, L., Renaud, A., Zimmer, L., " DMD algorithms for experimental data processing in combustion", *Proceedings of the summer program*, Center for turbulence research, Stanford University, 2012.

[8] Drmac, Z., Mezic, I., Mohr, A., "Data driven modal decompositions : analysis and enhancements", *SIAM Journal on Scientific Computing*, Vol. 40, No. 4, 2018, pp. A2253–A2285.

[9] Chen, K. K., Tu, J. H., Rowley, C. W., "Variants of dynamic mode decomposition : boundary conditions, Koopman, and Fourier analyses", *Journal of Nonlinear Science*, Vol. 22, No. 6, 2012, pp. 887–915.

[10] Tu, J. H., “Dynamic mode decomposition : theory and applications”, PhD thesis n° T-3268, 2013, Princeton University

[11] Towne, A., Schmidt, O. T., Colonius, T.,” Spectral proper orthogonal decomposition and its relationship to dynamic mode decomposition and resolvent analysis”, *Journal of Fluid Mechanics,* Vol. 847, 2018, pp. 821–867.

[12] Hirsh, S. M., Harris, K. D., Kutz, J. N., Brunton, B. W.,” Centering data improves the dynamic mode decomposition”, 2019, URL: https://arxiv.org/pdf/1906.05973.pdf

[13] Seenivasaharagavan, G. S., Korda, M., Arbabi, H., Mezic, I., “Mean subtraction and more selection in dynamic mode decomposition”, 2021, URL: https://arxiv.org/pdf/2105.03607.pdf

[14] Tissot, G., Cordier, L.,Benard, N., Noack, B. R., “Analyse par « Dynamic Mode Decomposition » de mesures PIV obtenues pour le sillage d’un cylindre circulaire en régime turbulent” , 13ème congrès francophone de techniques laser, Rouen, 2012.

[15] Bagheri, S., “Koopman-mode decomposition of the cylinder wake”, *Journal of Fluid Mechanics,* Vol. 726, 2013, pp. 821-867.

[16] Mezic, I., “Analysis of Fluid Flows via Spectral Properties of the Koopman Operator”, *Annual Revue of Fluid Mechanics,* Vol. 45, 2013, pp. 357–378.

[17] Hua, J.-C., Gunaratne, G. H., Talley, D. G., Gord, J. R., Roy, S., “Dynamic-mode decomposition based analysis of shear coaxial jets with and without transverse acoustic driving”, *Journal of Fluid Mechanics,* Vol. 790, 2016, pp. 5–32.

[18] Pascal, C., *Vibrations et acoustique 2*, ENSIM 2A, 2008-2009, URL : http://perso.univ-lemans.fr/~jcpascal/Cours/ENSIM2A_Vibrations&Acoustique_2.pdf

[19] Refloch, A., Courbet, B., Murrone, A., Villedieu, P., Laurent, C., Gilbank, P., Troyes, J., Tesse, L., Chaineray, G., Dargaud, J.-P., Quemerais, E., Vuillot, F., “CEDRE Software”, *ONERA – Aerospace Lab Journal*, Vol. 2, No. 11, 2011.

[20] Scherrer, D., Chedevergne, F., Grenard, P., Troyes, J., Murrone, A., Montreuil, E., Vuillot, F., Lupoglazoff, N., Huet, M., Sainte-Rose, B., Thorigny, P., Bertier, N., Lamet, J.-M., Le Pichon, T., Radenac, E., Nicole, A., Matuszewski, L., Errera, M., “Recent CEDRE Applications”, *ONERA – Aerospace Lab Journal*, Vol. 2, No. 13, 2011.